ISSN 1068-3755, Surface Engineering and Applied Electrochemistry, 2012, Vol. 48, No. 2, pp. 133–140. © Allerton Press, Inc., 2012.

Hardness and Electrochemical Behavior of Ceramic Coatings on CP Titanium by Pulsed Laser Deposition[1]

C. Sujaya and H. D. Shashikala

Department of Physics, National Institute of Technology Karnataka, Surathkal, Srinivasnagar, 575025, Karnataka, India
e-mail: sujayachendel@gmail.com

Received June 21, 2011; in final form, December 28, 2011

Abstract—Thin films of alumina and silicon carbide are deposited on titanium substrate by the pulsed laser deposition technique using Nd: YAG laser. Deposited films are characterized using x-ray diffraction, scanning electron microscopy, energy-dispersive x-ray spectroscopy, absorption spectroscopy and nanoindentation. Film hardness of the ceramic coating is found to be high compared to that of the substrates. Corrosion behavior of substrates after ceramic coating is studied in 3.5% NaCl solution by potentiodynamic polarization and electrochemical impedance spectroscopy measurements. Experimental results show an increase in corrosion resistance of titanium after being coated with a ceramic material.

DOI: 10.3103/S1068375512020147

INTRODUCTION

Titanium and its alloys have a wide range of applications in the fields of aerospace, chemical industry, marine and biomedical devices because of the combination of properties such as high strength-to-weight ratio, resistance to corrosion, and excellent biocompatibility [1, 2]. However, titanium shows poor tribological properties, which include high unstable friction coefficients and high wear rates [3]. The corrosion resistance of titanium can strongly decrease when a local mechanical abrasion removes the protective oxide film formed due to oxidation of the surface layer [4]. Surface treatments and coatings are practical approaches used to extend the lifetime of components and structures, since the surface is the most important part of an engineering component [4]. To improve the behavior of a surface, it is usually coated with ceramic materials. Thin ceramic coating is effective in enhancing and controlling the surface mechanical properties of engineering materials [5]. Thin films of alumina (Al_2O_3) and silicon carbide (SiC) are among the attractive materials to be used as a protective coatings so as to improve the lifetime or the performance of metallic substrates when exposed to aggressive environments [6]. These coatings have excellent optical properties, high mechanical strength and hardness, wear resistance, corrosion resistance [7, 8] and can be produced by many chemical and physical vapor deposition techniques. One of them, Pulsed Laser Deposition (PLD), is considered to be a flexible, simple and easily controllable method for producing thin films [9].

In the present study, adhesive films of Al_2O_3 and SiC are obtained using PLD technique on the fine polished titanium substrate at 450°C. Usually thicker ceramic films are deposited at higher temperatures, over 600°C. In our studies adhesive films of about 0.5 μm thickness are deposited at a lower temperature (450°C). As a result, an appreciable increase in both microhardness and corrosion resistance after coating has been observed. Processing parameters like laser fluence, substrate target distance, and substrate temperature during the deposition are standardized by multiple trials. Composite microhardness of Al_2O_3 and SiC coatings on commercially pure (CP) titanium substrate was measured using the Knoop indenter. The film hardness of both materials was separated from the composite hardness using a model based on that of Johnson and Hogmark, after including the indentation size effect (ISE) [10, 11], while comparing its values with those obtained with nanoindentation technique. Corrosion behavior of the coated substrate is studied using 3.5% NaCl solution by potentiodynamic polarization and electrochemical impedance spectroscopy (EIS) measurements.

EXPERIMENTAL

Substrate Preparation

The CP titanium was the substrate material used. The substrates were sequentially polished with SiC waterproof abrasive paper from 320 grit to 1500 grit size and with Al_2O_3 suspension of 1, 0.5, 0.3 μm size to an average roughness (R_a) of 40 nm. The fine polished surfaces were cleaned with acetone in the ultrasonic bath for 20 minutes before the deposition of the coating on the substrate.

The experimental setup consisted of a Q-switched Nd:YAG laser system, a focusing lens and a target

[1] The article is published in the original.

(SiC or Al_2O_3) placed inside the vacuum chamber, perpendicular to the laser beam. The experiments were carried out in vacuum of 10^{-4} torr. The laser system worked in the TEM00 mode and generates fundamental pulses at 1064 nm wavelength. The laser pulses were characterized by the duration of 7 ns and the repetition rate of 10 Hz. A laser beam of the energy of 135 mJ per pulse was focused to 0.1 cm diameter using a spherical lens of the focal length 50 cm, impinged onto the rotating target. Sintered Al_2O_3 and SiC pellets of thickness 0.4 cm and diameter 4 cm were used as targets. The rotation speed of 40 rotations-per-minute was used to avoid the crater formation. The incident angle between the laser beam and the target surface was kept at 45°. To obtain a uniform film thickness, the substrate was placed at 8 cm distance from the target surface. The ablation was carried out in vacuum under the pressure of 10^{-3} Pa, and at a substrate temperature of 450°C.

Measurement Techniques

Stylus profilometer was used to measure the film thickness. Optical absorption measurements were performed on Al_2O_3 and SiC coated on the optically flat glass substrate at room temperature using UV-Visible spectrophotometer. The X-ray diffraction (XRD) analysis was carried out by utilizing CuK_α radiation on ceramic coated substrates.

The hardness measurements were performed with the Knoop diamond pyramidal indenter by measuring the length of the rombohedral impression. Loads of 25 to 500 gm were employed at a dwell time of 10 seconds. At each load 10–12 indentations were made on the sample surface. The average microhardness at each load was calculated.

Direct determination of true film hardness of the thin films is not possible when the indentation depth is more than 10% of the total film thickness. In our studies, the true film hardness H_{fo} was determined using a model based on the area, i.e., area "law-of mixture," approach. It was originally proposed by Jonsson and Hogmark [10] for the Vickers indentation and later it was adapted to the geometrical configuration of the Knoop indenter [12]. The following equation is used for film hardness measurement in the Jonsson and Hogmark model

$$H_f = H_s + \frac{(H_c - H_s)}{2ct(t/l) - c^2(t^2/l^2)}, \qquad (1)$$

where c is constant, depending on the indenter geometry and the behavior (brittle or soft) of the material, l is the indentation depth, t is the film thickness, and H is the hardness. The subscripts c, f and s are related to the composite, film and the substrate, respectively. Usually, the measured hardness varies with load due to the indentation size effect (ISE) which was not taken into account in the Jonsson and Hogmark model. However, this model can be improved by incorporating ISE effect taking into account a linear relation between hardness and reciprocal indentation depth [10–12]. To obtain the true hardness of the film, the hardness variation with the applied load is written as

$$H_c = H_{\text{so}_s} + \frac{(B_c + 2ct(H_{fo} - H_{so})}{L}, \qquad (2)$$

where $c = 2.908$ (for the brittle film on the soft surface) or $c = 5.538$ (for the soft film on the soft surface) [13]; H_{fo} and H_{so} are the absolute hardness of the film and the substrate, respectively; B_s is a coefficient; L is the indentation diagonal length. The values of B_s and of the intercept H_{so} were determined from the study of the apparent Knoop hardness as a function of the inverse indentation diagonal L for the substrate. The film hardness obtained from the above model was compared with the film hardness obtained using nanoindentation method.

Generally, it is not possible to measure the properties of a thin film independent of the substrate, using conventional testing equipment, unless coating is very thick. In such cases nanoindenter is used. A common feature of this technique is that it continuously monitors load and displacement as the indentation is produced. The feature of a continuous depth and load recording allows thin film properties to be obtained directly from the data without measuring indentation diagonals. The data were analyzed with the Oliver and Pharr method [14].

The corrosion behavior of the coated and uncoated substrates were studied using the Tafel polarization studies by immersing samples in 3.5% NaCl solution in open air and at room temperature, using potentiostat/galvanostat PCI 4G750-47065 from Gamry Instruments Inc. All electrochemical measurements were performed using a conventional three-electrode cell, with a platinum plate as an auxiliary electrode and a saturated calomel electrode (SCE) as a reference electrode. The exposed area to the corrosive medium was 1 cm^2. The sample was cleaned in distilled water before loading to the sample holder. The sample was placed in such a way that the Luggin capillary of the reference electrode was close to the working electrode. This arrangement was used in all tests. An open circuit potential (E_{ocp}) or the steady state potential was maintained to study the potentiodynamic polarization. After getting the stable open circuit potential, the upper and the lower potential limits of the linear sweep voltmetry were set at ±250 mV, with respect to the E_{ocp}. The sweep rate was 1 mV/s. The Tafel plot was drawn using electrochemical data. The corrosion potential (E_{corr}) and the corrosion current density (i_{corr}) were deduced from the Tafel plot (log I vs E plot). The corrosion current density was obtained using the Stern–Geary equation [15]

$$i_{\text{corr}} = B/R_{\text{p}}, \qquad (3)$$

where $B = b_a b_c/2.303(b_a + b_c)$ where B is called the Stern–Geary constant, b_a and b_c are the Tafel slopes

for the anodic and cathodic reactions, respectively, and R_p is the polarization resistance expressed in $\Omega\,cm^2$. The corrosion rate (CR) was calculated from the Faraday law [16] using the following equation

$$CR(\mu m/y) = (3.27 i_{corr} EW)/d, \quad (4)$$

where EW is the equivalent weight of the testing material in grams and d is the density of testing sample in gm/cm^3. By substituting the value of i_{corr}, CR was calculated.

The EIS is considered to be one of the most important techniques for the investigation of the electrochemical behavior of passive films. Impedance measurements were conducted using a frequency response analyzer (FRA). The spectrum was recorded in the frequency range 10 mHz–300 KHz. The applied alternating potential had the root-mean-square amplitude of 10 mV. After each experiment, the impedance data was displayed as Nyquist and Bode plots. The Nyquist plot is a plot of imaginary impedance (Z'') versus real (Z'). From the Nyquist diagram it is possible to obtain the value of both the resistance, i.e., the electrolyte resistance (R_s), at high frequencies and charge transfer resistance (R_{ct}) at low frequencies. The Bode plot is a plot of $\log|Z|$ versus $\log f$ (magnitude plot), and phase angle (θ) versus $\log f$(phase plot), where $\log|Z|$ is the absolute impedance and f is the frequency. The advantage of the Bode plot is that the data for all the measured frequencies are displayed along with the impedance values. Furthermore, the frequency dependence of the phase angle indicates whether one or more time constants occur, which could be used to determine equivalent circuit parameters. A circuit description code (CDC) was assigned for the acquired data and the acquired data are curve fitted and analyzed using ZSimpWin software.

RESULTS AND DISCUSSION

Optical Characterization and XRD of Coating

Adhesive coatings of Al_2O_3 and SiC were obtained on the titanium substrate by using the standardized parameters mentioned in the previous section. The optical band gap energy and the Urbach energy calculations for SiC and Al_2O_3 coated on optically flat glass substrates were carried out using optical absorption data. The Tauc power law is used to obtain the optical band gap energy (E_g) [17]. Details of optical band gap energy and Urbach energy calculation are discussed in [18]. The E_g values are found to be 3.32 eV for Al_2O_3 and 2.07 eV for SiC film. These values are found to match with the reported values of 3.2 eV for Al_2O_3 [19] and 2–2.9 eV for SiC [20]. Generally, amorphous films have lower band gap energy compared to that of crystalline films.

The coated films investigated in the present work are amorphous in nature. This is confirmed by optical absorption data. At a longer wavelength in the spectrum, there is an absorption tail described by the Urbach exponential law [21], which describes the amorphous nature of the film. The Urbach energy is found to be 1.49 eV for Al_2O_3 and 1.39 eV for SiC films. These values for SiC and Al_2O_3 confirm that the obtained films are amorphous in nature. Absence of sharp XRD peaks (Fig. 1) also confirms that those films are amorphous in nature.

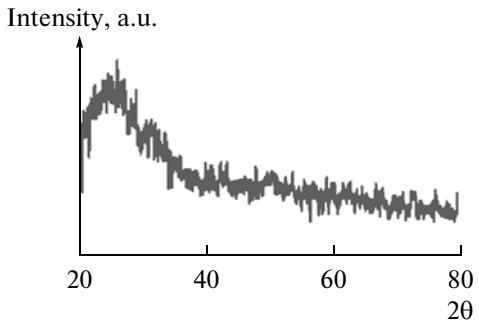

Fig. 1. XRD pattern of amorphous Al_2O_3 films.

Hardness Measurements

Figure 2 shows the inverse dependence of the measured composite film-substrate hardness on the diagonal indentation for Al_2O_3 and SiC coatings on titanium. A least-square fit to the plots of the Eq. (2) results in the slope $[(B)_{\downarrow}c = B_{\downarrow}s + 2ct(H_{\downarrow}fo - H_{\downarrow}so)]$. The value of c was chosen depending on whether the film is brittle or soft, since the nature of the films will be different from their bulk material. This value was 2.908 for the brittle film and 5.538 for the soft one [13, 22]. Two different methods were used here to verify whether the film was brittle or soft. The first was using Meyerâ's index number calculated from the Meyer law. This relates the load (P) and the indentation diagonal length L as $P = kL^n$

$$\log P = \log k + n \log L, \quad (5)$$

where k is the material constant and n is Meyer's index. In order to calculate the value of n, a graph, which is a straight line, was plotted between $\log P$ and $\log L$ (Figs. 3a, 3b). The slope of the straight line gives the value of n. According to Onitsch [23], n should lie between 1 to 1.6 for hard materials and above 1.6 for softer materials. The values of n obtained in the present study are listed in Table 2; they indicate the coating to be soft in nature. From the above reasoning, assuming the film to be soft, the c value is selected as $c = 5.538$. Using the value of B_s and H_{so} of the substrate, the intrinsic hardness of the films is calculated using Eq. 2. The slope of the straight line obtained by plotting H_c versus $1/L$ (Fig. 2) is used to calculate the intrinsic film hardness H_{fo}. The intrinsic hardness of the coated films is listed in Table 1. The film hardness is more than that of the substrate.

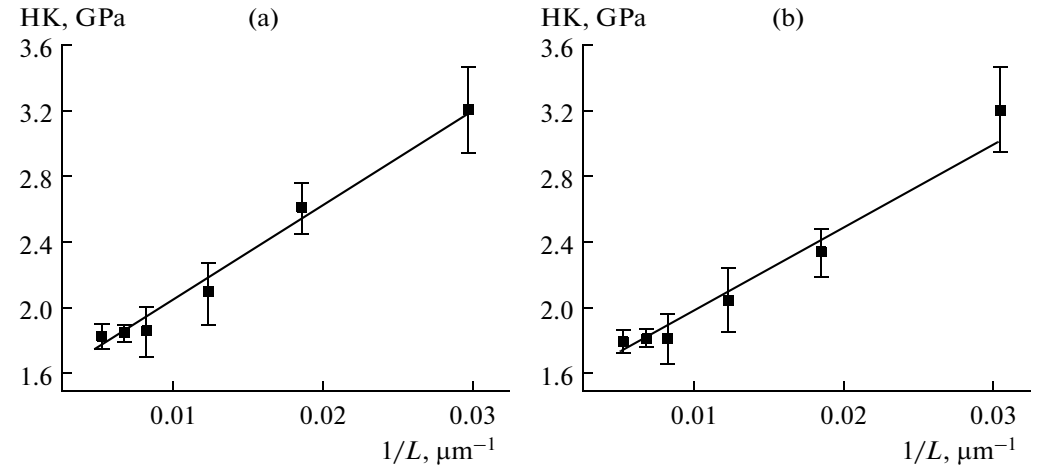

Fig. 2. Knoop hardness variation with 1/L on (a) Al_2O_3 and (b) SiC coated film on titanium.

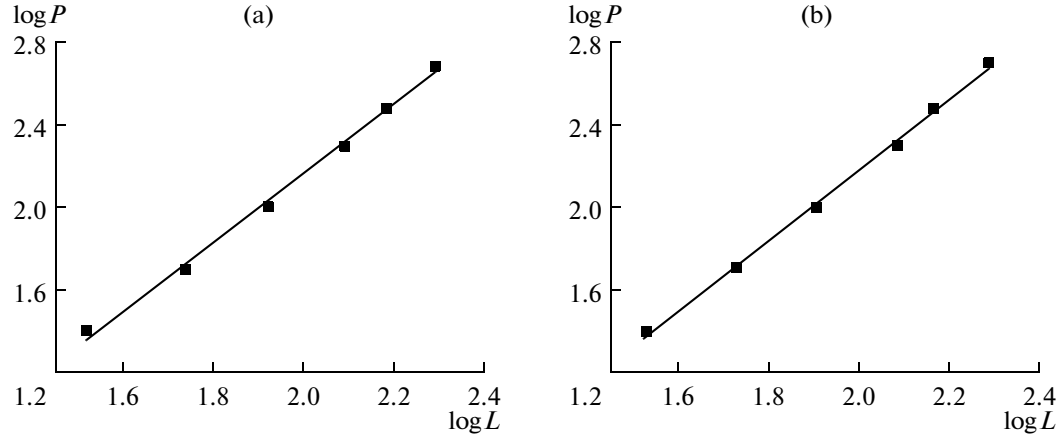

Fig. 3. Graph between log P variations with log L: (a) SiC film; (b) Al_2O_3 film.

Nanoindentation measurements were performed on the surface of titanium substrates both uncoated and coated with Al_2O_3 and SiC, in order to determine the hardness of coating. An indentation was carried out at the peak load of 1000 μN. The difference in hardness of the two samples was clearly evidenced by the difference in the depth obtained at the maximum load. The uncoated sample exhibited a larger indentation depth at the maximum load. In order to find the intrinsic hardness of the coated film, an indentation depth should be ten times less than that of the film thickness. The load was selected in such a way that its indentation depth was less than 0.05 μm on the coated substrate. The absence of kickbacks and elbows in the unloading curve of Al_2O_3 or SiC coated titanium substrate (Fig. 4) indicates the absence of substrate effect in the nanoindentation data. So, it can be concluded that the hardness obtained from nanoindentation is solely due to surface film. Similar observations were made in [24] while studying the effect of the substrate on Cu films. Table 2 compares the hardness values obtained using a mathematical model and the nanoin-

Table 1. Hardness data of coatings on titanium

Coating material	t (μm)	B_s (GPa m^{-1})	B_c (GPa m^{-1})	$2c$	H_{so} (GPa)	H_{fo} (GPa)
Al_2O_3	0.5	37.37	56.012	11.076	1.69	4.0
SiC	0.5	37.37	56.85	11.076	1.69	5.2

dentation method for Al_2O_3 and SiC films of the thickness 0.5 μm on the titanium substrate. It can be seen that the two values are in good agreement.

Potentiodynamic Polarization Measurements

The Tafel plots obtained for titanium, uncovered or covered with Al_2O_3 and SiC coatings of the thickness (t) 0.5 μm in 3.5% NaCl solution at 30°C are shown in Fig. 5. The corrosion potential (E_{corr}), the corrosion current density (i_{corr}) and the corrosion rate are deduced from the Tafel (log i vs. E) plots. Their values are listed in Table 3. For the titanium substrate, the i_{corr} is about 5.060 nA/cm^2 which decreases to 0.255 nA/cm^2 for Al_2O_3 coatings and to 2.860 nA/cm^2 for SiC coatings. The corrosion rate is directly proportional to i_{cor} The *CR* was found to reduce drastically after ceramic coating. Alumina coated substrates exhibit excellent corrosion resistance. With Al_2O_3 coating, the CR reduced six-fold compared to that of uncovered titanium, whereas with SiC coating the CR reduced five-fold compared to that of uncovered titanium. Improvement in the corrosion resistance of the substrate after ceramic coating is due to the fact that ceramic coating passivates the surface of the substrate and prevents the corrosion attack by the electrolyte. Generally, in physical vapor deposited coatings, electrolytes enter into the substrate through the defects like pores and micro cracks and cause the corrosion of the substrate [25]. The protective coatings must fulfill the two main requirements to achieve the remarkable effect on corrosion resistance. These are: a strong adhesion to the substrate, and a low density of pores and cracks. The absence of pores and micro cracks, complete surface coverage and good adhesion of the ceramic film coating to the substrate obtained by PLD technique enhances the corrosion resistance of the substrate. The enhanced CR of coatings on titanium in the present study indicates that the coated films are having negligible concentration of pores and cracks.

Table 2. Comparison of hardness values obtained using a model and nanoindentation method

Material	Meyer's index (n)	Thickness of the film (t) (μm)	Hardness (GPa)	
			From Model	Nano-indentation
Al_2O_3 on titanium	1.69	0.5	4.0	4.34
SiC on titanium	1.71	0.5	5.2	5.69

Table 3. Potentiodynamic polarization measurements

	Titanium	SiC	Al_2O_3
b_a (V/decade)	680 e-3	266e-3	363e-3
b_c (V/decade)	93 e-3	98e-3	136e-3
i_{corr} (nA/cm^2)	5.06	2.86	0.255
E_{corr} (mV)	−463.0	−369.0	−372.0
Corrosion rate (μmpy)	43.68	37.96	7.139
R_p (MΩ cm^2)	7.02	10.9	168

Electrochemical Impedance Spectroscopy Studies

Figures 6 and 7 present the impedance response of titanium and titanium with Al_2O_3 and SiC coatings, as the Nyquist and Bode plots, respectively. The EIS data obtained from these plots are listed in Table 4. The Nyquist plot shows an unfinished semicircle, which is attributed to the charge transfer controlled reaction

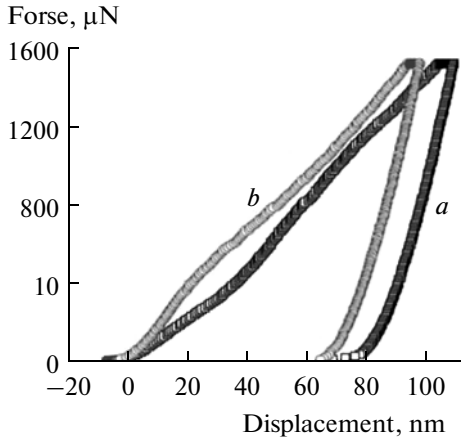

Fig. 4. Load variations with nanoindentation depth (*a*) Al_2O_3 and (*b*) SiC coating on titanium.

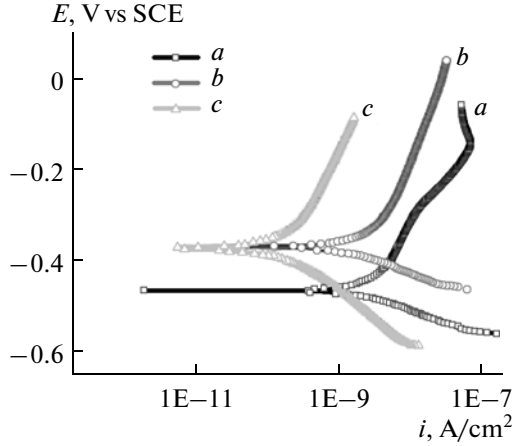

Fig. 5. Potentiodynamic polarization curves of (*a*) Al_2O_3 coated titanium; (*b*) titanium and (*c*) SiC coated titanium.

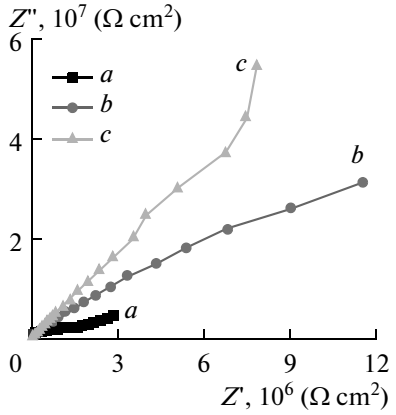

Fig. 6. Nyquist plot of the (*a*) titanium; (*b*) SiC and (*c*) Al_2O_3 coatings.

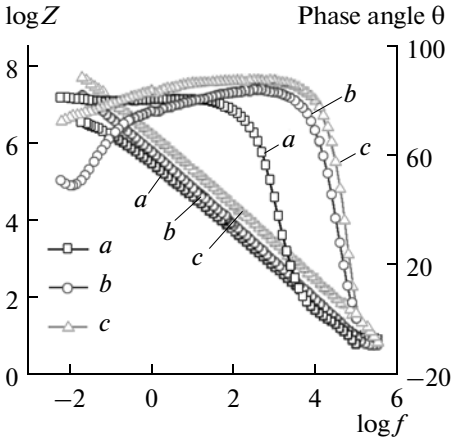

Fig. 7. Bode plots of (*a*) titanium; (*b*) SiC and (*c*) Al_2O_3 coatings.

[26]. The Bode plot of log*f* versus phase angle showed that the phase angle approaches 90°. It remains constant between the higher and lower frequency range (mHz-, KHz) suggesting that a highly stable film is formed on the surface [27].

The simplified equivalent circuits are shown in Fig. 8. The values of the solution resistance (R_s), charge-transfer resistance (R_{ct}), pore resistance (R_p), and the total capacitance (Q) of the constant phase element (CPE) are listed in Table 4. The R_{ct} increases in the following order: the titanium substrate, SiC

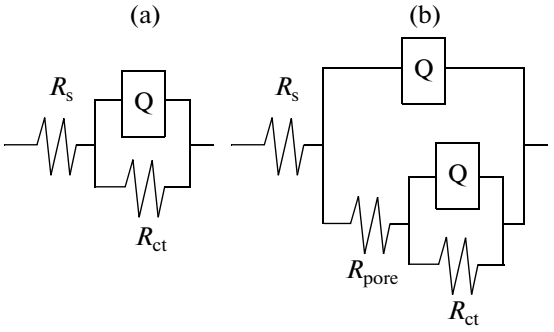

Fig. 8. (a) equivalent circuit to fit the electrochemical impedance data of the titanium substrate and (b) equivalent circuit to fit the electrochemical impedance data of the coated substrate.

coated titanium, Al_2O_3 coated titanium, which shows that the latter of the three has the highest corrosion resistance. The values of R_{ct} strongly depend on the passive film characteristics and are an indication of the corrosion of materials. This supports the results obtained using potentiodynamic polarization measurements. Figure 7 (log|*Z*| versus log*f*) shows that the absolute impedance increases in the same order as mentioned above. The equivalent circuit for titanium is shown in Fig. 8a. It consists of a double layer capacitance, which is parallel to the charge transfer resistance, both of which are in series with the solution resistance between the working electrode (WE) and the tip of the Luggin capillary. The double layer capacitance provides information about the polarity and the amount of charge at the substrate/electrolyte interface. The capacitance is replaced with the constant phase element (CPE) for a better quality fit. The CPE accounts for the deviation from an ideal dielectric behavior. *Q* stands for the constant phase element. This element is written in admittance form as

$$Y(w) = Y_0(jw)^m, \quad (6)$$

where Y_0 is an adjustable parameter used in the nonlinear least squares fitting and *m* is also an adjustable parameter that always lies in between 0.5 and 1. The value of *m* is obtained from the slope of log|*Z*| versus log*f* plot (Fig. 7). The phase angle (θ) can vary between 90° (for a perfect capacitor ($m = 1$)) and 0° (for a perfect resistor ($m = 0$)). The CDC for the equivalent circuit proposed for titanium is *R* (*Q*) *R*. When the sample is immersed in the electrolyte, the defects in the coating provide the direct diffusion path

Table 4. EIS data obtained by equivalent circuit simulation of SiC and Al_2O_3 coatings

Sample	R_s (Ω cm^2)	Q_{dl}–Y_0 (μF/cm^2)	n_{dl}	R_{ct} (MΩ cm^2)	Q_{coat}–Y_0 (μF/cm^2)	n_c	R_{pore} (MΩ cm^2)
Titanium	5.4	0.3066	0.8	0.779			
Titanium/SiC	10	0.107	0.8	974	0.0605	0.76	12.2
Titanium/Al_2O_3	8.26	0.342	0.97	59	0.57	0.57	18.1

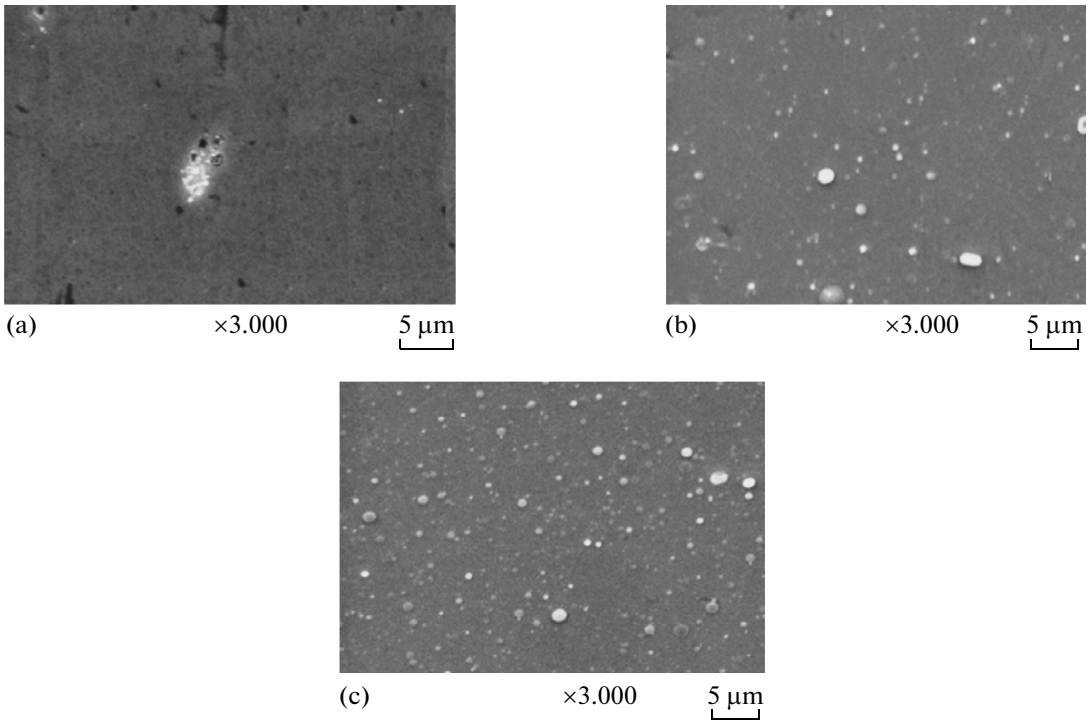

Fig. 9. Surface topography of the (a) titanium substrate; (b) SiC; (c) Al_2O_3 coated substrate surface.

for the corrosive media. In this process, the galvanic corrosion cells are formed and the localized corrosion dominates the corrosion process. In such cases, an electrochemical interface can be divided into two subinterfaces: electrolyte/coating and electrolyte/substrate. The proposed equivalent circuit for such a system is shown in Fig. 8b. The parameters in the equivalent circuit R_p and Q_c are related to the properties of the coating and the electrolyte/coating interface reactions. R_{ct} and Q_{dl} are related to the charge-transfer reaction at the electrolyte/substrate interface. The CDC of the proposed equivalent circuit for the coated sample is R (Q[R (QR)]). From the EIS data given in Table 4, it is seen that Q_c decreases from SiC coating to Al_2O_3 coating indicating that SiC coatings have relatively more pores and less dense microstructure than Al_2O_3 coatings.

Scanning Electron Microscopy Studies

After the corrosion testing, the surface topography of the uncoated and the coated systems were studied by the Scanning Electron Microscopy (SEM). The corrosion pits were observed on the uncoated titanium after the corrosion test (Fig. 9a). Corrosion pits are not found in Al_2O_3 and SiC coated samples, (Figs. 9b, 9c). Pits are formed as a result of a corrosion attack on the uncoated surface.

The improvement in the corrosion resistance is due to adherent thin Al_2O_3 film coating deposited on the surface of the substrate which will not allow the direct contact of the electrolyte with the substrate. EDX analysis indicates the presence of sodium (Na) and Chlorine in the regions where the pits are formed. Similar conclusion can be drawn in corrosion behavior of SiC coated titanium.

CONCLUSIONS

In this paper we have studied the influence of adhesive thin films of Al_2O_3 and SiC coatings on the titanium substrate deposited by the PLD technique using Nd:YAG laser. It has been shown that hardness and corrosion resistance are improved when the coatings are deposited by the PLD. The intrinsic film hardness separated from the composite hardness, using a model based on the area law of mixtures, is nearly equal to the film hardness measured using nanoindentation technique. The potentidynamic polarization and the EIS measurements showed that Al_2O_3 and SiC coatings exhibit better corrosion resistance as compared to that of the substrate due to the negligible pores and cracks in the film. The EIS measurements over a wide frequency range also indicate good stability of the coated films.

ACKNOWLEDGMENTS

The authors would like to thank Indian Space Research Organization (ISRO) for financial assistance in carrying out this research work and Vikram Sarab-

hai Space Centre (VSSC), Trivandrum for supplying substrate materials.

REFERENCES

1. Dong, H. and Bell, T., Enhanced Wear Resistance of Titanium Surfaces by a New Thermal Oxidation Treatment, *Wear,* 2000, vol. 238, no. 2, pp. 131–137.
2. Mahmoud, S.S., Electroless Deposition of Nickel and Copper on Titanium Substrates: Characterization and Application, *Journal of Alloys and Compounds*, 2009, vol. 472, pp. 595–601.
3. Dearnley, P.A., Dahm, K.L., and Çimenolu, H., The Corrosion-wear Behavior of Thermally Oxidized CP–Ti and Ti–6A1–4V, *Wear*, 2004, vol. 256, no. 5, pp. 469–479.
4. Richard, C., Kowandy, C., Landoulsi, J., Geetha, M., and Ramasawmy, H., Corrosion and Wear Behavior of Thermally Sprayed Nano Ceramic Coatings on Commercially Pure Titanium and Ti-13Nb-13Zr Substrates, *International Journal of Refractory Metals and Hard Materials*, 2010, vol. 28, no. 1, pp. 115–123.
5. Berasategui, E.G. and Page, T.F., The Contact Response of thin SiC-coated Silicon Systems-characterization by Nanoindentation, *Surface and Coatings Technology*, 2003, vols. 163–164, pp. 491–498.
6. Sella, C., Lecoeur, J., Sampeur, Y., and Catania, P., Corrosion Resistance of Amorphous Hydrogenated SiC and Diamond-like Coatings Deposited by r.f.-plasma-enhanced Chemical Vapour Deposition, *Surface and Coatings Technology*, 1993, vol. 60, no. 3, pp. 577–583.
7. Xuguo Huai, Shihai Zhao and Wandeng Li, Corrosion Resistance of Al_2O_3 Coating on a Steel Substrate, *Journal of Ceramic Processing Research*, 2009, vol. 10, no. 5, pp. 618–620.
8. Katharria, Y.S., Sandeep Kumar, Ram Prakash, Choudhary, R.J., Singh, F., Phase, D.M., and Kanjilal, D., Characterizations of Pulsed Laser Deposited SiC Thin Films, *Journal of Non-Crystalline Solids*, 2007, vol. 353, pp. 4660–4665.
9. Zhu, T.J., Lu, L., and Lai, M.O., Pulsed Laser Deposition of Lead-zirconate-titanate thin Films and Multilayered Heterostructures, *Applied Physics A*, 2005, vol. 81, no. 4, pp. 701–714.
10. Jönsson, B. and Hogmark, S., Hardness Measurements of thin Films, *Thin Solid Films,* 1984, vol. 114, no. 3, pp. 257–269.
11. Guillemot, G., Isot, A., and Chikot, D., Comments on the Paper "Modification of Composite Hardness Models to Incorporate Indentation Size Effects in thin Films," Beegan, D., Chowdhury, S., and Laugier, M.T., *Thin Solid Films*, 2008, 516, 3813–3817. Thin Solid Films. 2010, vol. 518, no. 8, pp. 2097–2101.
12. Iost, A., Knoop Hardness of thin Coatings, *Scripta Materialia*, 1998, vol. 39, no. 2, pp. 231–238.
13. Torregrosa, F., Barrallier, L., and Roux, L., Phase Analysis, Microhardness and Tribological Behaviour of Ti–6A1–4V after Ion Implantation of Nitrogen in Connection with its Application for Hip-joint Prosthesis, *Thin Solid Films*, 1995, vol. 266, no. 2, pp. 245–253.
14. Oliver, W.C. and Pharr, G.M., An Improved Technique for Determining Hardness and Elastic-modulus Using Load and Displacement Sensing Indentation Experiments, *Journal of Materials Research*, 1992, vol. 7, pp. 1564–1583.
15. Sastri, S., *Corrosion Inhibitors-Principles and Applications*, Chichester: John Willy and Sons, 1998.
16. Dean, S.W., Jr., *Electrochemical Methods of Corrosion Testing, Electrochemical Techniques for Corrosion*, Baboian, R., Ed., Houston, Texas: NACE, 1977, pp. 52–60.
17. Tauc, J., *Optical Properties of Solids*, Abels, F., Ed., North-Holland, Amsterdam, 1972.
18. Sujaya, C., Shashikala, H.D., Umesh, G., and Hegde, A.C., Hardness and Electrochemical Behavior of Ceramic Coatings on Inconel, *Journal of Electrochemical Science and Engineering*, 2011 (in press).
19. Rose, V., Podgursky, V., Costina, I., and Franchy, R., Growth of Ultra-thin Amorphous Al_2O_3 Films on CoAl(100), *Surface Science*, 2003, vol. 541, no. 3, pp. 128–136.
20. Park, Y.J., Park, Y.W., and Chun, J.S., The Bond Structures and Properties of Chemically Vapour Deposited Amorphous SiC, *Thin Solid Films*, 1998, vol. 166, pp. 367–374.
21. Urbatch, F., The Long Wavelength Edge of Photographic Sensitivity and of the Electronic Absorption of Solids, *Physics Review*, 1953, vol. 92, p. 1324.
22. Ferro, D., Barinov, S.M., Rau, V.J., Latini, A., Scandurra, R., and Brunetti, B., Vickers and Knoop Hardness of Electron Beam Deposited ZrC and HfC thin Films on Titanium, *Surface & Coatings Technology,* 2000, vol. 200, no. 17, pp. 4701–4707.
23. Onitsch, E.M., Micro-hardness Testing, *Mikroscopia*, 1941, vol. 2, p. 131.
24. Beegan, D., Chowdhury, S., and Laugier, M.T., Modification of Composite Hardness Models to Incorporate Indentation Size Effects in thin Films, *Thin Solid Films*, 2008, vol. 516, pp. 3813–3817.
25. Barshilia, H.C., Yogesh, K., and Rajam, K.S., Deposition of TiAlN Coatings Using Reactive Bipolar-pulsed Direct Current Unbalanced Magnetron Sputtering, *Vacuum*, vol. 83, no. 2, pp. 427–434.
26. Liu, L., Li, Y., and Wang, F., Influence of Microstructure on Corrosion Behavior of a Ni-Based Superalloy in 3.5 wt % NaCl, *Electrochemica Acta*, 2007, vol. 52, no. 25, pp. 7193–7202.
27. Tamilselvi, S. and Rajendran, N., Electrochemical Studies on the Stability and Corrosion Resistance of Ti–5Al–2Nb–1Ta Alloy for Biomedical Applications, *Trends in Biomaterials & Artificial Organs*, 2006, vol. 20, no. 1, pp. 49–52.